

Electrochemical and Physicochemical Characterizations of Butylsulfate-Based Ionic Liquids

I-Wen Sun¹, Yuan-Chung Lin², Bor-Kuan Chen³, Chung-Wen Kuo⁴, Chi-Chang Chen¹, Shyh-Gang Su¹, Pin-Rong Chen⁵, Tzi-Yi Wu^{5,*}

¹ Department of Chemistry, National Cheng Kung University, Tainan 70101, Taiwan

² Institute of Environmental Engineering, National Sun Yat-Sen University, Kaohsiung 804, Taiwan

³ Department of Materials Engineering, Kun Shan University, Tainan 710, Taiwan

⁴ Department of Chemical and Materials Engineering, National Kaohsiung University of Applied Sciences, Kaohsiung 80778, Taiwan

⁵ Department of Chemical and Materials Engineering, National Yunlin University of Science and Technology, Yunlin 64002, Taiwan

*E-mail: wuty@yuntech.edu.tw

Received: 22 June 2012 / Accepted: 14 July 2012 / Published: 1 August 2012

A series of butylsulfate-based ionic liquids (ILs) are prepared using butylsulfate anions with various cations, the influences of ring structural variations of cations on their thermal property, electrochemical window, density, viscosity, and ionic conductivity are investigated. Good electrochemical stability (ca. 4.7 V) of the butylsulfate-based ILs is confirmed by voltammetric measurements, and the incorporation of methyl group to replace acidic C-2 hydrogen atom of imidazolium cation or replace imidazolium unit by pyrrolidinium or tri(n-propyl)ammonium slightly increases the cathodic stability. The deviations between ILs and ideal KCl line in adjust Walden plot decreases significantly than those in general Walden plot owing to the adjusted Walden plot takes the difference of ion size into account.

Keywords: Ionic liquid, molten salt, conductivity, electrochemical window, Walden rule

1. INTRODUCTION

Over the past decade much attention has been given to ionic liquids (ILs), a class of compounds comprised only of ions, with melting points below 100 °C [1]. They are composed of organic cations and organic or inorganic anions and are called “designer solvents” because desired properties can be obtained by combination of their ions [2,3]. These ionic compounds are being explored as potential friendly-environmental solvents due to their negligible vapor pressure in comparison to traditional volatile organic solvents and they are widely used in various electrochemical devices, such as lithium

or electrochemical sensors [4-14], lithium-ion batteries [15-19], electrodeposition [20-24], dye-sensitized solar cells [25-29], fuel cell [30], and electrochemical capacitors [31,32].

Physicochemical properties of bulk ILs are of immense importance for electrochemical and engineering applications [33-43], for instance, viscosity of ILs has fundamental importance, as all the equations expressing the flow of fluids contain this important property and can provide information about various classes of fluids on molecular basis. Viscosity as a transport property has a significant impact on the rate of mass transport and thus is an important factor. Several chemicals and products characteristic can be largely determined by numerical values of viscosity. Temperature dependent viscosity of ILs is more complicated than many molecular solvents because most of them do not follow the typical Arrhenius behaviour. For instance, Okoturo *et al.* [44] presented a systematic study of viscosity of ILs and showed that the temperature variation of viscosity of ILs follows the Arrhenius equation or Vogel–Tamman–Fulcher (VTF) equation. With the aim of enhancing the understanding of unusual characteristics of RTILs, numerous studies on their thermophysical properties such as viscosity, density, ionic conductivity, molar conductivity, diffusion coefficient etc. have been carried out [45-49]. In the past several years, the most commonly studied ILs contain an imidazolium cation with varying heteroatom functionality. Imidazolium based ILs especially those based on the (PF_6^- , BF_4^- , or $[(\text{CF}_3\text{SO}_2)_2\text{N}]^-$) anion are considered historically the most important and commonly investigated. However, the hydrolytical instability of such anions has become obvious, and decomposition of these fluorinated anions leads to the formation of highly toxic and corrosive HF, the use of these ionic liquids will be limited [50]. Accordingly, the synthesis and application of halogen free ionic liquids is necessary. Several types of these ionic liquids are based on alkyl sulfonates, organoborates and alkyl sulfate anions. The most important properties of alkyl sulfate based ionic liquids are easily synthesis, using cheap alkylating agent, solvent free synthesis, high reaction rate, excellent purity, large scale synthesis, safe and nontoxic chemical, low viscosities, and low melting points [51]. In this work, several butylsulfate-based ILs are reported, and their physicochemical and electrochemical properties such as the density, viscosity, thermal property, ionic conductivity, and potential window are studied in detail.

2. EXPERIMENTAL

2.1. Materials and measurement

All starting materials were purchased from Aldrich, Lancaster, TCI, and Acros and used as received. The conductivity (σ) of the ILs was systematically measured with a conductivity meter LF 340 and a standard conductivity cell TetraCon 325 (Wissenschaftlich-Technische Werkstätten GmbH, Germany). The cell constant was determined by calibration after each sample measurement using an aqueous 0.01 M KCl solution. The density of the ILs was measured with a dilatometer, which was calibrated by measuring the density of neat glycerin at 30, 40, 50, 60, 70, and 80 °C. To measure the density, IL or binary mixture was placed into the dilatometer up to the mark, sealed the top of capillary tube, which was on the top of the dilatometer, and placed into a temperature bath for 10 min to allow

the temperature to equilibrate. The main interval between two marks in capillary tube is 0.01 cm^3 , and the minor interval between two marks is 0.001 cm^3 . From the correction coefficient of glycerin in capillary tube at various temperatures, we can calculate the density of neat IL or binary system by the expanded volume of liquid in capillary tube at various temperatures. Each sample was measured at least three times to determine an average value, and the values of the density are $\pm 0.0001 \text{ g mL}^{-1}$. The viscosities (η) of the ILs were measured using a calibrated modified Ostwald viscometer (Cannon-Fenske glass capillary viscometers, CFRU, 9721-A50) with inner diameters of $1.2 \pm 2\%$ mm. The viscometer was placed in a thermostatic water bath (TV-4000, TAMSON), in which the temperature was regulated to within $\pm 0.01 \text{ K}$. The flow time was measured with a stop watch capable of recording to 0.01 s . For each IL, the experimental viscosity was obtained by averaging three to five flow time measurements. The melting point of each IL was analyzed by using a differential scanning calorimeter (DSC, Perkin–Elmer Pyris 1) in the temperature range $-140 \text{ }^\circ\text{C}$ to a predetermined temperature. The sample was sealed in an aluminum pan, and then heated and cooled at a scan rate of $10 \text{ }^\circ\text{C min}^{-1}$ under a flow of nitrogen. The thermal data were collected during the second heating–cooling scan. The thermal stabilities were measured with TGA (Perkin–Elmer, 7 series thermal analysis system). The sample was heated at $20 \text{ }^\circ\text{C min}^{-1}$ from room temperature to $800 \text{ }^\circ\text{C}$ under nitrogen. The water content of the dried ILs was detected by a Karl–Fischer moisture titrator (Metrohm 73KF coulometer), and the values were less than 300 ppm. NMR spectra of synthetic ionic liquids were recorded on a BRUKER AV500 spectrometer in D_2O and calibrated with tetramethylsilane (TMS) as the internal reference. Cyclic voltammetry was performed at 25°C using an electrochemical workstation (CH instruments Inc., CHI, model 750A). The electrochemical cell consist a glassy carbon working electrode, a Pt wire counter electrode, and a Pt quasi-reference electrode. All electrochemical experiments were performed under a dry argon atmosphere to avoid the presence of oxygen and air humidity. The structures of the ILs studied in the present work are shown in Table 1.

2.2. Synthetic procedure of butylsulfate-based ILs

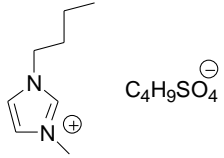
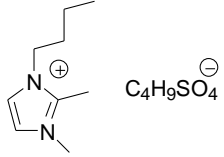
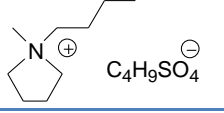
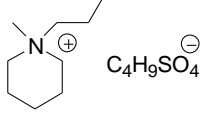
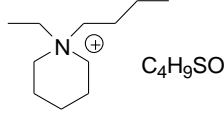
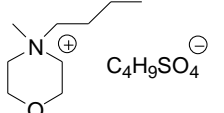
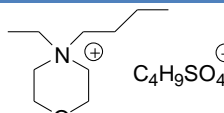
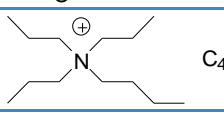
2.2.1. 1-Butyl-3-methyl-imidazolium butyl sulfate ([BMI][BuSO₄])

Dibutyl sulfate (75.7 g, 360 mmol) was added dropwise to a solution of equal molar amounts of 1-methylimidazole (29.56 g, 360 mmol) in 200 mL toluene, and then cooled in an ice-bath under nitrogen at a rate that maintained the reaction temperature below 313.15 K (highly exothermic reaction). The reaction mixture was stirred at room temperature for 4h. After the reaction stopped, the upper organic phase of the resulting mixture was decanted, and the lower ionic liquid phase was washed with ethyl acetate (4 x 70 mL). After the last washing, the remaining ethyl acetate was removed by rotavapor under reduced pressure. The IL obtained was dried by heating at (343.15 to 353.15) K and stirring under a high vacuum ($2 \times 10^{-1} \text{ Pa}$) for 48 h. In order to reduce the water content to negligible values (lower than 0.03 mass %), a vacuum ($2 \times 10^{-1} \text{ Pa}$) and moderate temperature (343.15 K) were applied to the IL for 2 days. The IL was kept in bottles under an inert gas.

Yield: 91 %. $^1\text{H NMR}$ (300 MHz, D_2O , ppm): 8.63 (s, 1H, imidazole hydrogen), 7.38 (d, 2H, imidazole hydrogen), 4.12 (t, 2H, N- CH_2CH_2), 3.97 (t, 2H, $-\text{CH}_2\text{SO}_4$), 3.81 (s, 3H, N- CH_3), 1.76 (m,

2H, N-CH₂CH₂-), 1.56 (m, 2H, -CH₂CH₂SO₄), 1.29 (m, 4H, N-CH₂CH₂CH₂- and -CH₂CH₂CH₂SO₄), 0.83 (m, 6H, N-CH₂CH₂CH₂CH₃ and CH₃CH₂CH₂CH₂SO₄). Elem. Anal. Calcd. for C₁₂H₂₄N₂O₄S: C, 49.29 %; H, 8.27 %; N, 9.58 %. Found: C, 49.38 %; H, 8.32 %; N, 9.50 %.

Table 1. The denominations and chemical structures of butylsulfate-based ILs.

Ionic liquids	Structure
[BMI][BuSO ₄]	
[DMBI][BuSO ₄]	
[PyrMB][BuSO ₄]	
[PipMB][BuSO ₄]	
[PipEB][BuSO ₄]	
[MorMB][BuSO ₄]	
[MorEB][BuSO ₄]	
[TPABu][BuSO ₄]	

2.2.2. 1-Butyl-2,3-dimethyl-imidazolium butyl sulfate [DMBu][BuSO₄]

Yield: 88 %. ¹H NMR (300 MHz, D₂O, ppm): 7.27 (d, 2H, imidazole hydrogen), 4.02 (t, 2H, N-CH₂-), 3.96 (t, 2H, -CH₂SO₄), 3.68 (s, 3H, N-CH₃), 2.50 (s, 3H, C-CH₃), 1.70 (m, 2H, N-CH₂CH₂-), 1.56 (m, 2H, -CH₂CH₂SO₄), 1.27 (m, 4H, N-CH₂CH₂CH₂- and -CH₂CH₂CH₂SO₄), 0.83 (m, 6H, N-CH₂CH₂CH₂CH₃ and CH₃CH₂CH₂CH₂SO₄). Elem. Anal. Calcd. for C₁₃H₂₆N₂O₄S: C, 50.96 %; H, 8.55 %; N, 9.14 %. Found: C, 50.88 %; H, 8.48 %; N, 9.02 %.

2.2.3. 1-Butyl-1-methylpyrrolidinium butyl sulfate [PyrMB][BuSO₄]

Yield: 91 %. ¹H NMR (300 MHz, D₂O, ppm): 3.95 (t, 2H, -CH₂SO₄), 3.38 (m, 4H, N-CH₂-), 3.21 (m, 2H, N-CH₂-), 2.92 (s, 3H, N-CH₃), 2.10 (m, 4H, N-CH₂CH₂-), 1.67 (m, 2H, -CH₂CH₂SO₄), 1.55 (m, 2H, N-CH₂CH₂-), 1.28 (m, 4H, N-CH₂CH₂CH₂- and -CH₂CH₂CH₂SO₄), 0.82 (m, 6H, N-CH₂CH₂CH₂CH₃ and CH₃CH₂CH₂CH₂SO₄). Elem. Anal. Calcd. for C₁₃H₂₉NO₄S: C, 52.85 %; H, 9.89 %; N, 4.74 %. Found: C, 52.68 %; H, 9.79 %; N, 4.65 %.

2.2.4. 1-Butyl-1-methylpiperidinium butyl sulfate [PipMB][BuSO₄]

Yield: 86 %. ¹H NMR (300 MHz, D₂O, ppm): 3.98 (t, 2H, -CH₂SO₄), 3.22 (m, 6H, N-CH₂-), 2.93 (s, 3H, N-CH₃), 1.79 (m, 4H, N-CH₂CH₂- and -CH₂CH₂SO₄), 1.61 (m, 6H, N-CH₂CH₂- and N-CH₂CH₂CH₂-), 1.31 (m, 4H, N-CH₂CH₂CH₂- and -CH₂CH₂CH₂SO₄), 0.85 (m, 6H, N-CH₂CH₂CH₂CH₃ and CH₃CH₂CH₂CH₂SO₄). Elem. Anal. Calcd. for C₁₄H₃₁NO₄S: C, 54.34 %; H, 10.10 %; N, 4.53 %. Found: C, 54.18 %; H, 10.03 %; N, 4.39 %.

2.2.5. 1-Butyl-1-ethylpiperidinium butyl sulfate [PipEB][BuSO₄]

Yield: 82 %. ¹H NMR (300 MHz, D₂O, ppm): 3.96 (t, 2H, -CH₂SO₄), 3.28-3.12 (m, 8H, N-CH₂-), 1.76 (m, 4H, N-CH₂CH₂-), 1.57 (m, 6H, N-CH₂CH₂-, N-CH₂CH₂CH₂-, and -CH₂CH₂SO₄), 1.29 (m, 4H, N-CH₂CH₂CH₂- and -CH₂CH₂CH₂SO₄), 1.17 (t, 3H, N-CH₂CH₃), 0.84 (m, 6H, N-CH₂CH₂CH₂CH₃ and CH₃CH₂CH₂CH₂SO₄). Elem. Anal. Calcd. for C₁₅H₃₃NO₄S: C, 55.69 %; H, 10.28 %; N, 4.33 %. Found: C, 55.46 %; H, 10.21 %; N, 4.21 %.

2.2.6. 4-Butyl-4-methylmorpholinium butyl sulfate [MorMB][BuSO₄]

Yield: 89 %. ¹H NMR (300 MHz, D₂O, ppm): 3.98 (m, 6H, -CH₂SO₄ and OCH₂-), 3.39 (m, 6H, N-CH₂-), 3.10 (s, 3H, N-CH₃), 1.68 (m, 2H, -CH₂CH₂SO₄), 1.57 (m, 2H, N-CH₂CH₂-), 1.32 (m, 4H, N-CH₂CH₂CH₂- and -CH₂CH₂CH₂SO₄), 0.86 (m, 6H, N-CH₂CH₂CH₂CH₃ and CH₃CH₂CH₂CH₂SO₄). Elem. Anal. Calcd. for C₁₃H₂₉NO₅S: C, 50.13 %; H, 9.39 %; N, 4.50 %. Found: C, 50.98 %; H, 9.36 %; N, 4.37 %.

2.2.7. 4-Butyl-4-ethylmorpholinium butyl sulfate [MorEB][BuSO₄]

Yield: 80 %. ¹H NMR (300 MHz, D₂O, ppm): 3.98 (m, 6H, -CH₂SO₄ and OCH₂-), 3.44 (m, 6H, N-CH₂-), 3.33 (t, 2H, N-CH₂-), 1.60 (m, 4H, N-CH₂CH₂- and -CH₂CH₂SO₄), 1.35-1.21 (m, 7H, N-CH₂CH₃, N-CH₂CH₂CH₂-, and -CH₂CH₂CH₂SO₄), 0.86 (m, 6H, N-CH₂CH₂CH₂CH₃ and CH₃CH₂CH₂CH₂SO₄). Elem. Anal. Calcd. for C₁₄H₃₁NO₅S: C, 51.66 %; H, 9.60 %; N, 4.30 %. Found: C, 51.45 %; H, 9.62 %; N, 4.18 %.

2.2.8. *N,N,N*-tripropylbutan-1-aminium butyl sulfate [TPABu][BuSO₄]

Yield: 88 %. ¹H NMR (300 MHz, D₂O, ppm): 3.96 (t, 2H, -CH₂SO₄), 3.06 (m, 8H, N-CH₂CH₂-), 1.58 (m, 10H, N-CH₂CH₂- and -CH₂CH₂SO₄), 1.28 (m, 4H, N-CH₂CH₂CH₂- and -CH₂CH₂CH₂SO₄), 0.85 (m, 15H, N-CH₂CH₂CH₃, N-CH₂CH₂CH₂CH₃, and CH₃CH₂CH₂CH₂SO₄). Elem. Anal. Calcd. for C₁₇H₃₉NO₄S: C, 57.75 %; H, 11.12 %; N, 3.96 %. Found: C, 57.56 %; H, 11.03 %; N, 3.87 %.

3. RESULTS AND DISCUSSION

3.1. Thermal Property

Table 2 summarizes the melting points and glass phase transitions along with the thermal decomposition onset temperatures and physicochemical quantities of density (ρ), viscosity (η), conductivity (σ), and concentration (C) at 30 °C. The thermal properties of the eight ILs were investigated using thermogravimetric analysis (TGA) and differential scanning calorimetry (DSC), and their TGA traces are shown in Fig. 1. As shown in Fig. 1, the eight ILs show one stage decomposition behavior, all of the thermal decomposition onset temperatures (5 % weight loss) are above 209 °C, with the highest being found for [PyrMB][BuSO₄] (277 °C). The T_d of these ILs has some relationship with the cations, the thermal stability of cations is pyrrolidinium > imidazolium > piperidinium and morpholinium. These ionic liquids have potential usage as alternative to conventional organic solvents due to their thermal stability. The glass temperature (T_g) and melting temperature (T_m) can be obtained from the DSC thermograms during the programmed reheating step. From the DSC, there are three endothermic peaks for [DMBI][BuSO₄], which indicated that it probably has the transition from solid to solid at -38 and 16 °C and melting at 47 °C. The T_m of a compound is associated with the strength of its crystal lattice, which is controlled by intermolecular forces, molecular symmetry, and degrees of the freedom of the molecule.

Table 2. Physical and thermal properties of butylsulfate-based ILs.

Ionic liquid	$M_w /$ g mol ⁻¹	$T_g /$ °C	$T_{s-s} /$ °C	$T_m /$ °C	$T_d /$ °C	$\rho /$ g cm ⁻³	$C /$ mol dm ⁻³	$\eta /$ mPa s	$\sigma /$ mS cm ⁻¹	$\Lambda /$ S cm ² mol ⁻¹
[BMI][BuSO ₄]	292.40	-86	---	-25	257	1.1268	3.85	270	0.62	0.160
[DMBI][BuSO ₄]	306.42	-89	-38, 16	47	245	---	---	---	---	---
[PyrMB][BuSO ₄]	295.44	-86	---	---	277	1.1199	3.79	675	0.32	0.084
[PipMB][BuSO ₄]	309.47	-90	---	55	227	---	---	---	---	---
[PipEB][BuSO ₄]	323.49	-79	---	43	214	---	---	---	---	---
[MorMB][BuSO ₄]	311.44	-67	---	---	210	1.1458	3.68	4318	0.033	0.0089
[MorEB][BuSO ₄]	325.47	-64	---	19	209	---	---	---	---	---
[TPABu][BuSO ₄]	353.56	-63	---	75	223	1.0289	2.91	4034	0.025	0.0087

^a Density (ρ), concentration (C), viscosity (η), conductivity (σ) and molar conductivity (Λ) are measured at 30 °C.

^b Decomposition temperature (T_d) of 5 % weight loss.

The highest melting points are exhibited for [TPABu][BuSO₄], likely due the easier packing of both cation and anion, e.g., leading to remarkable ion lattice energy values, since their high symmetry [52].

3.2. Density, viscosity and conductivity

The values of ρ (g cm⁻³) for four RTILs ([BMI][BuSO₄], [PyrMB][BuSO₄], [MorMB][BuSO₄], and [TPABu][BuSO₄]) decreased with increasing temperature were shown in Fig. 2. A linear relationship ($r > 0.998$) with temperature was obtained for the four RTILs. The experimental density was correlated with the following equation:

$$\rho = b + aT \quad (1)$$

where a , b , and T are the coefficient of volume expansion (g cm⁻³ K⁻¹), the density at 0 K (g cm⁻³), and temperature (K), respectively. The best fit parameters of Eq. (1) were summarized in Table 3. As shown in Table 2, cyclic amine-based IL [PyrMB][BuSO₄] (1.1199 g cm⁻¹ at 30 °C) has higher density than tripropylamine-based IL [TPABu][BuSO₄] (1.0289 g cm⁻¹ at 30 °C), this can be attributed to tight intermolecular packing between cyclic amine-based cation and butylsulfate. The morpholinium-based ionic liquid has a higher density ([MorMB][BuSO₄]: $\rho = 1.1458$ g cm⁻³ at 30 °C) than that of pyrrolidinium-based ionic liquids ([PyrMB][BuSO₄] ($\rho = 1.1199$ g cm⁻¹ at 30 °C)). This shows that higher-density liquids have a denser structure. In morphiline-based RTIL, the electron rich oxygen part likely interacts with other organic cations.

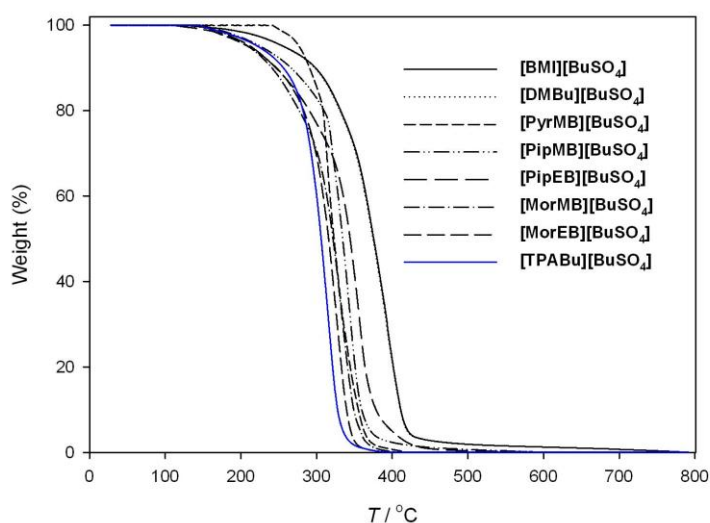


Figure 1. Thermogravimetric trace for the butylsulfate-based ionic liquids.

Imidazolium-based IL [BMI][BuSO₄] ($\rho = 1.1268 \text{ g cm}^{-3}$ at 30 °C) has higher density than pyrrolidinium-based IL [PyrMB][BuSO₄] ($\rho = 1.1199 \text{ g cm}^{-3}$ at 30 °C) due to planar imidazolium unit facilitates to form π - π stacking between two imidazolium units.

Table 3. The adjustable parameters of density ($\rho = b + aT$) and VTF equation parameters of viscosity

$$(\eta^{-1} = \eta_o \exp[\frac{B}{(T-T_o)}]) \text{ for ILs.}$$

Ionic liquids	ρ			η			
	b	$10^4 a$	R^{2a}	$\eta_o / \text{mPa s}$	T_o / K	B / K^b	R^{2a}
[BMI][BuSO ₄]	1.3309	-6.739	0.9994	0.1451	174.5	968.1	0.999
[PyrMB][BuSO ₄]	1.2936	-5.739	0.9997	0.2248	183.4	958.3	0.999
[MorMB][BuSO ₄]	1.3474	-6.654	0.9987	0.204	195	1076	0.999
[TPABu][BuSO ₄]	1.2362	-6.841	0.9987	0.169	210.6	931.1	0.999

^a Correlation coefficient.

^b Activation energy (kJ mol⁻¹).

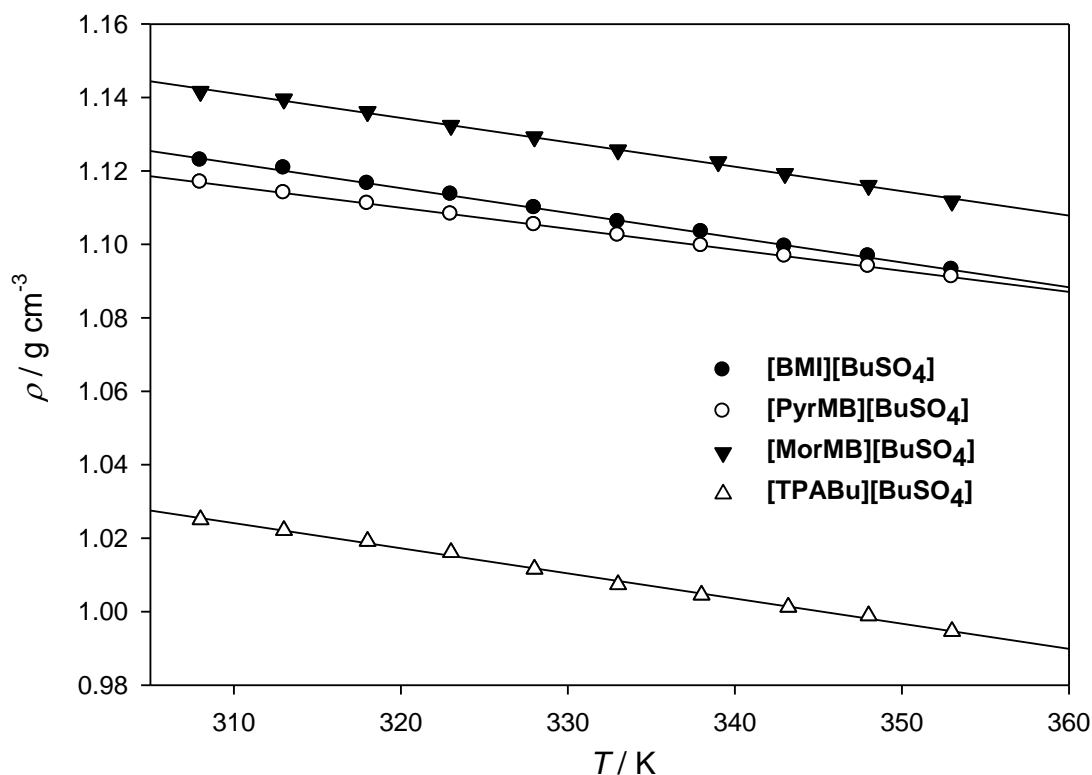


Figure 2. Temperature dependence of density data for the ILs.

Viscosity is an important property of ionic liquids used as electrolyte solutions in electrochemical studies due to its influence on the mass transport rate in electrolyte. As shown in Fig. 3, the viscosities were found to decrease with increasing temperature. Therefore, the viscosity of ionic

liquids can be adjusted to meet the needs of applications by changing temperature. The temperature effect on the viscosity of the ILs can be fitted by the Arrhenius equation which is a simplified version of Eyring's absolute rate theory [53]:

$$\eta = \eta_{\infty} \exp\left[\frac{-E_{a,\eta}}{RT}\right] \quad (2)$$

where η_{∞} , $E_{a,\eta}$, R , and T were a constant for given liquid, the activation energy for the viscous flow, the gas constant, and the absolute temperature, respectively.

Due to the deviation from a strictly linear Arrhenius-type relationship (eq 2) and the physical background just mentioned, it is much better to fit $\eta - T$ data pairs using Vogel–Tamman–Fulcher (VTF) equation and modified Vogel–Tamman–Fulcher (modified VTF) equation. The most commonly used equation to correlate the variation of viscosity with temperature is the Arrhenius-like law, but according to Seddon *et al.*[54] the Arrhenius law can generally be applied when the cation presents only a limited symmetry. If this is not the case, Vogel–Tamman–Fulcher (VTF) and modified equation Vogel–Tamman–Fulcher are recommended [54]. The modified VTF equation can be expressed:

$$\eta = \eta_0 \cdot T^{0.5} \exp\left[\frac{B}{T - T_0}\right] \quad (3)$$

and the VTF equation can be presented as:

$$\eta = \eta_0 \cdot \exp\left[\frac{B}{T - T_0}\right] \quad (4)$$

where η_0 , B , and T_0 are adjustable parameters, the best-fit η_0 (cP), B (K), and T_0 (K) parameters are given in Table 3.

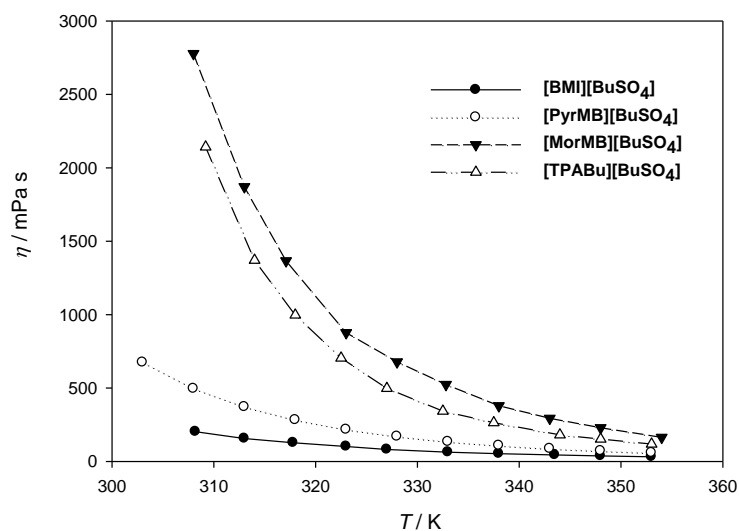


Figure 3. Dynamic viscosity (η) as a function of temperature for ILs.

The viscosity of ILs is essentially influenced by the strength of their van der Waals interactions, the hydrogen bonding ability, and the planarity of molecular structure, a relatively high viscosity for [MorMB][BuSO₄] and [TPABu][BuSO₄] can be attributed to hydrogen bonding formation between the oxygen atom of morpholinium unit and sulfate, and the long length of the propyl side chain in cation, respectively. A viscosity comparison of [BMI][BuSO₄] and [PyrMB][BuSO₄] indicates the presence of a more planar structure (imidazolium unit) is known to result in less viscosity because the planarity allows relatively facile slip between molecules.

The E_a , ΔS , and ΔH values of four butylsulfate-based RTILs evaluated using the slope ($-E_a/R$) of the η vs. T plot are summarized in Table 4. The absolute values of E_a , ΔS , and ΔH for the ILs are in the order: [BMI][BuSO₄] ($E_a = 38.02$ kJ mole⁻¹, $|\Delta S| = 333.29$ J mole⁻¹ K⁻¹, and $\Delta H = 40.74$ kJ mole⁻¹) < [PyrMB][BuSO₄] ($E_a = 43.35$ kJ mole⁻¹, $|\Delta S| = 343.23$ J mole⁻¹ K⁻¹, and $\Delta H = 46.06$ kJ mole⁻¹) < [MorMB][BuSO₄] ($E_a = 55.76$ kJ mole⁻¹, $|\Delta S| = 369.40$ J mole⁻¹ K⁻¹, and $\Delta H = 58.48$ kJ mole⁻¹) < [TPABu][BuSO₄] ($E_a = 62.44$ kJ mole⁻¹, $|\Delta S| = 392.38$ J mole⁻¹ K⁻¹, and $\Delta H = 65.15$ kJ mole⁻¹).

Table 4. The E_a , ΔS and ΔH evaluated by Eyring equation and the relationships of η vs. T , σ vs. T , and Λ vs. T .

Ionic liquids	η			σ			Λ		
	$E_a/$ kJ mole ⁻¹	$\Delta S/$ J mole ⁻¹ K ⁻¹	$\Delta H/$ kJ mole ⁻¹	$E_a/$ kJ mole ⁻¹	$\Delta S/$ J mole ⁻¹ K ⁻¹	$\Delta H/$ kJ mole ⁻¹	$E_a/$ kJ mole ⁻¹	$\Delta S/$ J mole ⁻¹ K ⁻¹	$\Delta H/$ kJ mole ⁻¹
[BMI][BuSO ₄]	38.02	-333.29	40.74	37.62	-133.48	34.90	38.16	-142.92	35.44
[PyrMB][BuSO ₄]	43.35	-343.23	46.06	28.51	-169.04	25.79	28.97	-178.60	26.25
[MorMB][BuSO ₄]	55.76	-369.40	58.48	58.85	-87.27	56.13	59.37	-96.38	56.66
[TPABu][BuSO ₄]	62.44	-392.38	65.15	57.94	-92.28	55.22	58.54	-99.18	55.83

The conductivity of an ionic liquid is of vital importance if it is to be considered as a supporting electrolyte in electrochemical devices. The temperature dependence of conductivity for these ILs is depicted in Fig. 4, an increase in temperature leads to an increase in the ion mobility. The temperature vs. electrical conductivity (σ) dependence for an ionic liquid is generally represented by the Arrhenius-type equation:

$$\sigma = \sigma_{\infty} \exp\left[\frac{-E_{a,\sigma}}{k_B T}\right] \quad (5)$$

where σ_{∞} is the electrical conductivity at infinite temperature, E_a is the activation energy (e.g., needed for an ion to hop in a free hole), k_B is the Boltzmann constant, and T is the absolute temperature. However, the conduction behavior of most of the IL samples does not follow the exponential dependence with the inverse of the temperature given by the Eq. (5). In fact, the observed conductivity vs. temperature curvature is accounted for a VTF-type equation:

$$\sigma = \sigma_{\infty} \exp\left[\frac{-E_{a,\sigma}}{k_B (T - T_g)}\right] \quad (6)$$

where T_g represents the glass transition temperature. Or

$$\sigma = \sigma_o \exp\left[\frac{-B'}{(T-T_o)}\right] \quad (7)$$

where σ_o , B' , and T_o were the fitting parameters. Table 5 summarizes VTF fitting parameters obtained by fitting the conductivity vs. temperature data of Figure 4 with the VTF-type Eq. (7), four butylsulfate-based ILs were very well fit by the VTF model over the temperature range studied. For these salts with butylsulfate anion, the conductivity generally decreased in the order: [BMI][BuSO₄] > [PyrMB][BuSO₄] > [MorMB][BuSO₄] > [TPABu][BuSO₄], this cation tendency is similar to that observed in the corresponding imidazolium and aliphatic quaternary ammonium salts and is the combined result of several competing factors that affect the conductivity, including the viscosity, formula weight, and ion size, as explained in previous reports [55].

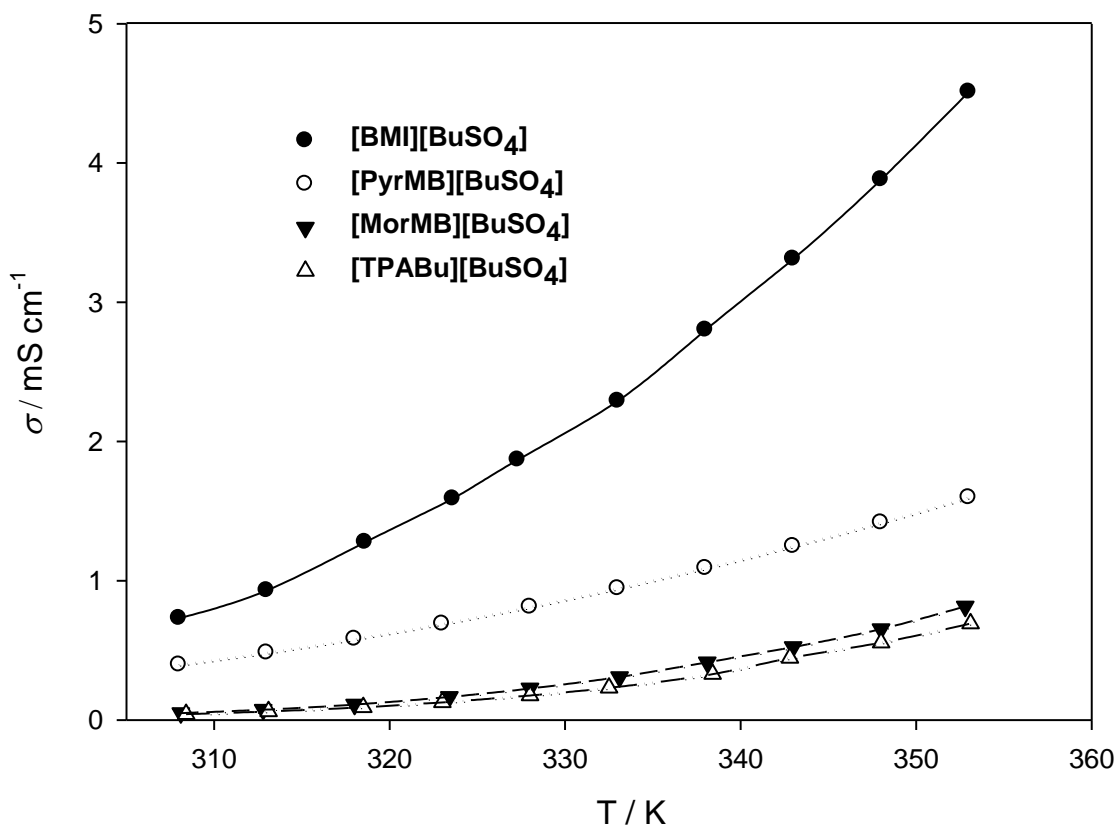


Figure 4. Dependence of specific conductivity (σ) on temperature for the ILs.

For the relationship of σ vs. T , the E_a , ΔS , and ΔH values evaluated using the slope ($-E_a/R$) of the Arrhenius and Eyring equations for the ILs are summarized in Table 4. The E_a , ΔS , and ΔH values of the ILs show different tendency with viscosity and are in the order: [PyrMB][BuSO₄] < [BMI][BuSO₄] < [TPABu][BuSO₄] < [MorMB][BuSO₄].

Table 5. VTF equation parameters of conductivity ($\sigma = \sigma_0 \exp[\frac{-B'}{T-T_0}]$) and molar conductivity

$$(\Lambda = \Lambda_0 \exp[\frac{-B'}{T-T_0}]) \text{ for ILs.}$$

Ionic liquids	σ				Λ			
	σ_0 / S cm ² mol ⁻¹	T_0 /K	B' /K	R^{2a}	Λ_0 / S cm ² mol ⁻¹	T_0 /K	B' /K	R^{2a}
[BMI][BuSO ₄]	1054	174.8	954.2	0.999	308.5	174.3	973.7	0.999
[PyrMB][BuSO ₄]	114	170.2	780.1	0.999	35.1	168.3	812.5	0.999
[MorMB][BuSO ₄]	454	206.1	925.3	0.999	100.1	209.4	873.3	0.999
[TPABu][BuSO ₄]	136	217.1	737.4	0.999	107.7	207.7	897.8	0.999

^a Correlation coefficient.

Molar conductivity of the ILs Λ (S cm² mol⁻¹) was calculated by using the expression $\Lambda = \sigma M / \rho$, where M , σ , ρ are the respective equivalent weight, specific conductivity, and density of the ILs. The temperature dependence of molar conductivity for these ILs is depicted in Figure 5. The observed temperature dependences of molar conductivity are well fitted by the empirical VTF equation:

$$\Lambda = \Lambda_0 \exp\left[\frac{-B'}{T-T_0}\right] \quad (8)$$

where Λ_0 , B' , and T_0 are the fitting parameters. VTF fitting parameters of the molar conductivity for the ILs are summarized in Table 5. For the relationship of Λ vs. T , the E_a , ΔS , and ΔH values evaluated using the slope ($-E_a/R$) of the Arrhenius and Eyring equations for the ILs are summarized in Table 4. The E_a , ΔS , and ΔH values of the molar conductivity (Λ) have similar relationship with specific conductivity (σ).

The Walden rule provides a useful basis for organizing and classifying the ILs [56]. It is a relation between the molar conductivity, Λ , and the viscosity, η , of a solution, and summarizes in the following equation:

$$\Lambda \eta^\alpha = C \quad (9)$$

where C is a temperature-dependent constant, which is called the Walden product. α is the slope of the line in the Walden plot, which reflects the decoupling of the ions. The fitted α values of the ILs are given in Table 6. The parameter α reflects the difference of the activation energies of the ionic conductivity and viscosity. Another method that yields almost identical values of α is the ratio of the temperature-dependent activation energies for viscosity and molar conductivity, $E_{a,\Lambda}/E_{a,\eta}$. The activation energies are summarized in Table 4.

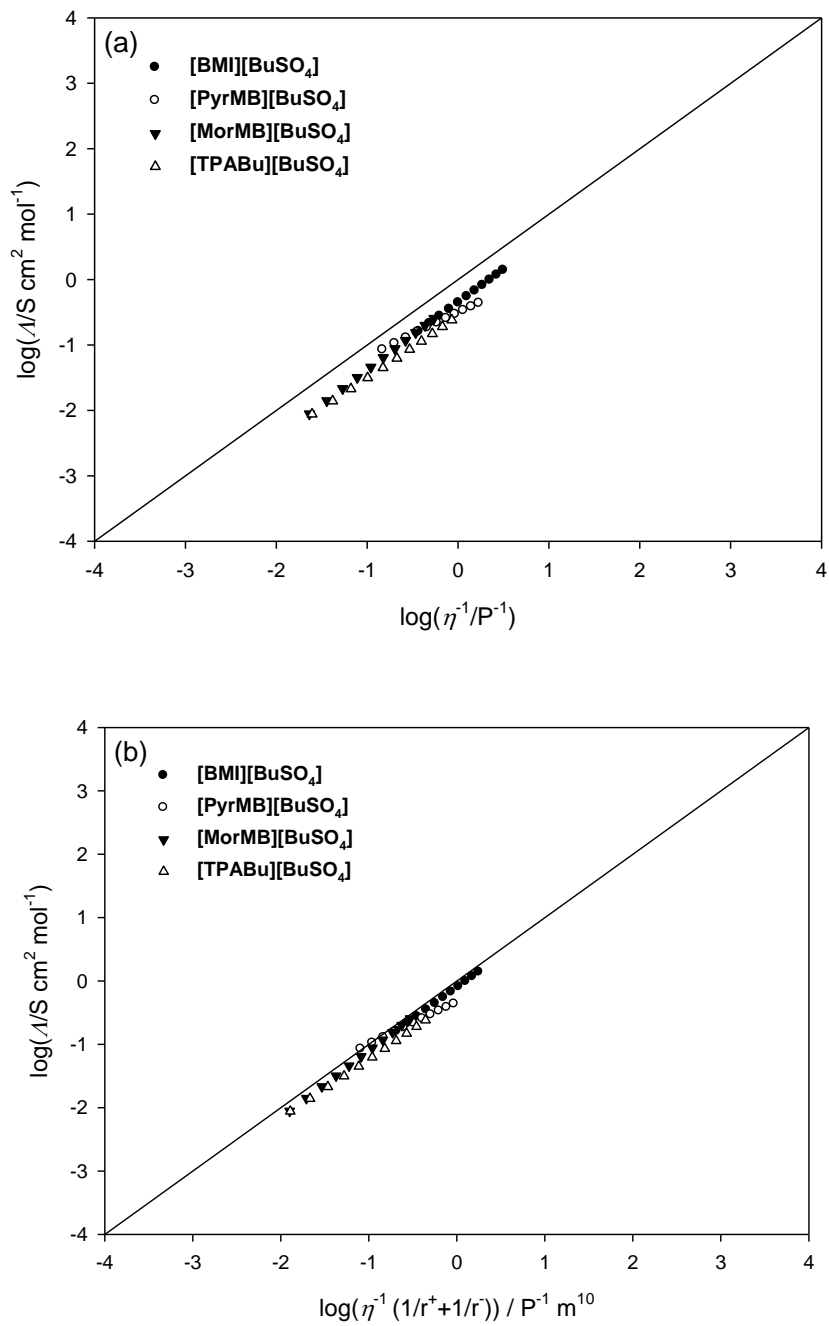


Figure 5. Dependence of molar conductivity (Λ) on temperature for the ILs.

Table 6 compares α_{\square} values calculated from the slopes of the Walden plots in Figure 6(a) with those calculated from the activation energies. The two methods for obtaining α_{\square} values are in very good agreement.

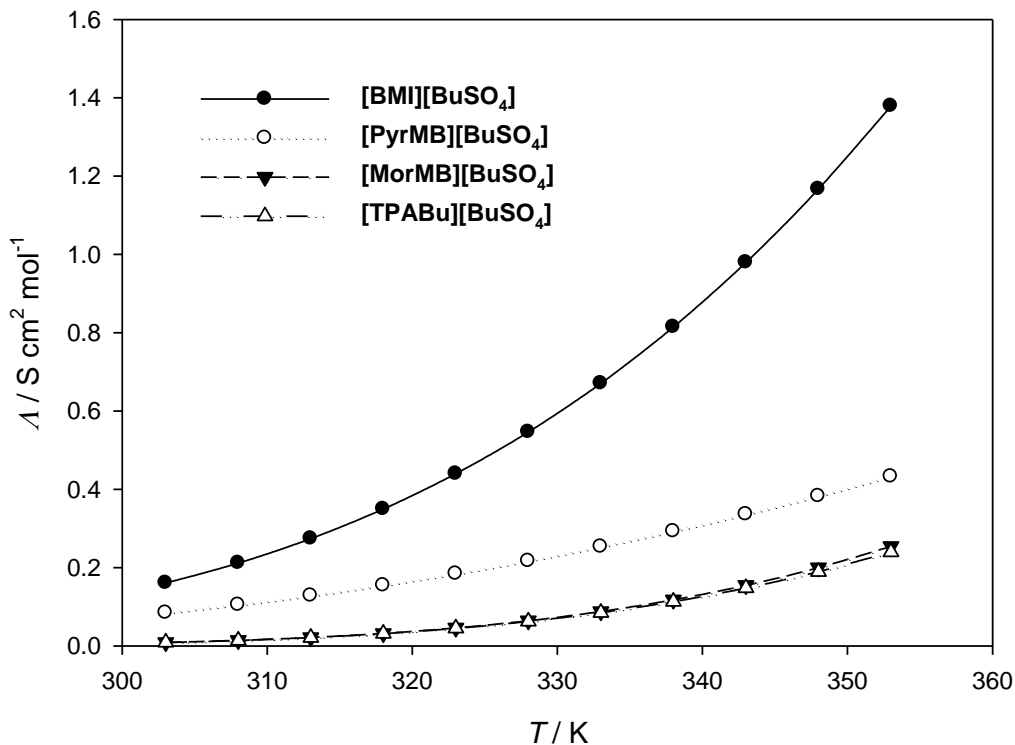


Figure 6. Walden plots for various ILs, where Λ is the equivalent conductivity and η^{-1} is the fluidity. The ideal line runs from corner to corner of a square diagram is generated from data obtained in aqueous KCl solution. (a) General Walden plot; (b) adjusted Walden plot of taking the difference in ion size into account.

Figure 6(a) shows the general Walden plot of four butylsulfate-based ILs, compare the discrepancy from the KCl ideal line of Walden plots, a relatively large deviation of the plots from the ideal Walden line is observed for [TPABu][BuSO₄], which suggests that ion–ion correlations in [TPABu][BuSO₄] is stronger, and more ion pairs or aggregates appeared in these two ILs [57].

The general Walden plot (Figure 6(a)) does not take into account the difference in ion size, an adjusted Walden plot defined by MacFarlane et al. [57] depicts a relationship of Λ and η as follows:

$$\Lambda = C\eta^{-1}\left[\frac{1}{r^+} + \frac{1}{r^-}\right] \tag{10}$$

Table 6. Comparison of the activation energies for the absolute viscosity, $E_{a,\eta}$, and equivalent conductance, $E_{a,\Lambda}$. α_{\square} is from the general Walden plots and α_{EA} is calculated from the ratio of the activation energies ($E_{a,\Lambda} / E_{a,\eta}$).

Ionic liquids	$E_{a,\eta} / \text{kJ mole}^{-1}$	$E_{a,\square} / \text{kJ mole}^{-1}$	α	α_{EA}
[BMI][BuSO ₄]	38.02	38.16	1.0037	1.0035
[PyrMB][BuSO ₄]	43.35	28.97	0.6683	0.6686
[MorMB][BuSO ₄]	55.76	59.37	1.0647	1.0645
[TPABu][BuSO ₄]	62.44	58.54	0.9375	0.9365

where C is constant and r^+ and r^- are the “effective” cation and anion sizes, respectively. The van der Waals (vdW) radii evaluated using Winmostar software [58] for [BMI], [PyrMB], [MorMB], [TPABu], and [BuSO₄] are 3.613, 3.814, 3.850, 4.320, and 3.512 Å, respectively. Figure 6(b) shows the adjusted Walden plot of taking the difference of ion size into account, the deviations between ILs and ideal KCl line in adjust Walden plot decreases significantly than those in general Walden plot. Four butylsulfate-based ILs are close to the ideal KCl line, suggesting a good ionization of these ILs.

3.3. Electrochemical stability

The electrochemical window is defined as the potential interval observed between the reduction potential of the organic cationic part and the oxidation potential of the anionic part of pure ILs. A wide electrochemical window makes ILs promising electrolytes for electrochemical applications. These butylsulfate-based ILs are swept to obtain cyclic voltammetric curve using a glassy carbon working electrode as shown in Figure 7, and the cathodic or anodic limiting potential of the ILs are summarized in Table 7, where the potential (V) were referenced to internal ferrocene (Fc)/ferricinium (Fc⁺) redox couple. The cathodic limiting potential of ILs is mainly ascribable to the reduction of the cation and is moderately affected by the nature of the anion, among the ILs studied, the ILs containing BMI⁺ cation show less cathodic stability, due to lower electrochemical stability of the imidazolium [59]. The incorporation of methyl group in acidic C-2 hydrogen atom of imidazolium cation or replace imidazolium unit with pyrrolidinium or morpholinium may influence the cathodic stability, as shown in Table 7, the values of cathodic limit potential of these ILs are scattered ranging from -2.65 to -2.93 V versus Fc/Fc⁺ couple, and increased in the order: |[BMI]⁺| < |[DMBI]⁺| < (|[MorMB]⁺| or |[TPABu]⁺|) < |[PyrMB]⁺|. This tendency suggests that introduce of methyl group to replace acidic C-2 hydrogen atom of imidazolium cation or replace imidazolium unit by pyrrolidinium or tri(n-propyl)ammonium slightly increases the cathodic stability. In the other hand, the anodic limiting potential of ILs is mainly ascribable to the oxidation of the butylsulfate anion and is moderately affected by the nature of the cation, and it is comparable to other sulfate-based ILs (anodic limit vs. Fc/Fc⁺ = 1.8 V [60]). The electrochemical windows for the ILs studied are ranging from about 4.47 V to 4.74 V, and decrease in the order: [PyrMB][BuSO₄] > ([MorMB][BuSO₄] and [TPABu][BuSO₄]) > [DMBI][BuSO₄] > [BMI][BuSO₄].

Table 7. Electrochemical windows of ionic liquids.

Ionic liquids	Cathodic limiting potential V vs. Fc/Fc ⁺	Anodic limiting potential V vs. Fc/Fc ⁺	Electrochemical Window V
[BMI][BuSO ₄]	-2.65	1.82	4.47
[DMBI][BuSO ₄]	-2.72	1.90	4.62
[PyrMB][BuSO ₄]	-2.93	1.81	4.74
[MorMB][BuSO ₄]	-2.86	1.83	4.69
[TPABu][BuSO ₄]	-2.84	1.85	4.69

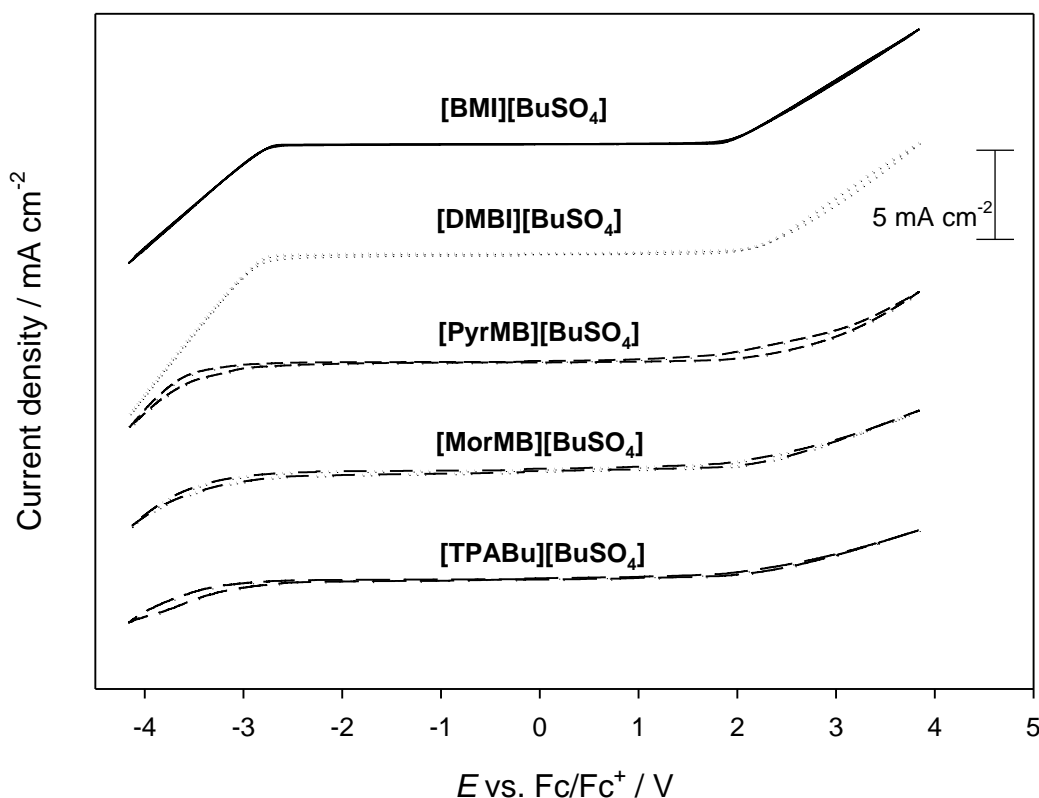


Figure 7. Cyclic voltammogram of ILs relative to Pt reference electrode, with glassy carbon working electrode and Pt counter electrode. Potential was calibrated using the redox potential of ferrocene/ferricenium (Fc/Fc^+) redox couple measured in each ionic liquid.

4. CONCLUSIONS

A series of ILs containing various imidazolium, cyclic ammonium, and tetraalkylammonium units as cation, and a butylsulfate unit as anion were synthesized. The resulting physicochemical properties show that the effect of cation identity is preponderant. Four butylsulfate-based ILs are liquid at room temperature and show good thermal stability. The butylsulfate-based ILs exhibit wide electrochemical windows of about 4.7 V, and 1,3-dialkylimidazolium salt shows the highest ionic conductivity and lowest viscosity among the butylsulfate-based ILs. The correlation between ionic conductivity and viscosity is based on the classical Walden rule; a relatively large deviation of the plots from the ideal Walden line is observed for the ILs without considering the ion size, whereas the deviation decreases significantly when the adjusted Walden plot is adopted. The α values of butylsulfate-based ILs calculated from the slopes of the Walden plots are compared to those calculated from the ratio of activation energies for viscosity and molar conductivity ($E_{a,\Lambda}/E_{a,\eta}$).

ACKNOWLEDGEMENTS

The authors would like to thank the National Science Council of the Republic of China for financially supporting this project.

References

1. R.D. Rogers, K.R. Seddon, *Ionic Liquids: Industrial Applications for Green Chemistry*, American Chemical Society, Washington, DC, 2003.
2. T. Torimoto, T. Tsuda, K. Okazaki, S. Kuwabata, *Adv. Mater.*, 22 (2010) 1196.
3. T.Y. Wu, S.G. Su, K.F. Lin, Y.C. Lin, H.P. Wang, M.W. Lin, S.T. Gung, I.W. Sun, *Electrochim. Acta*, 56 (2011) 7278.
4. M.R. Ganjali, H. Ganjali, M. Hosseini, P. Norouzi, *Int. J. Electrochem. Sci.*, 5 (2010) 967.
5. M.R. Ganjali, S. Aghabalazadeh, M. Rezapour, M. Hosseini, P. Norouzi, *Int. J. Electrochem. Sci.*, 5 (2010) 1743.
6. M. Pandurangachar, B.E.K. Swamy, B.N. Chandrashekar, O. Gilbert, S. Reddy, B.S. Sherigara, *Int. J. Electrochem. Sci.*, 5 (2010) 1187.
7. P. Norouzi, Z. Rafiei-Sarmazdeh, F. Faridbod, M. Adibi, M.R. Ganjali, *Int. J. Electrochem. Sci.*, 5 (2010) 367.
8. F. Faridbod, M.R. Ganjali, M. Pirali-Hamedani, P. Norouzi, *Int. J. Electrochem. Sci.*, 5 (2010) 1103.
9. M.R. Ganjali, M.H. Eshraghi, S. Ghadimi, S.M. Moosavi, M. Hosseini, H. Haji-Hashemi, P. Norouzi, *Int. J. Electrochem. Sci.*, 6 (2011) 739.
10. M.R. Ganjali, T. Poursaberi, M. Khoobi, A. Shafiee, M. Adibi, M. Pirali-Hamedani, P. Norouzi, *Int. J. Electrochem. Sci.*, 6 (2011) 717.
11. P. Norouzi, M. Hosseini, M.R. Ganjali, M. Rezapour, M. Adibi, *Int. J. Electrochem. Sci.*, 6 (2011) 2012.
12. M.R. Ganjali, M.R. Moghaddam, M. Hosseini, P. Norouzi, *Int. J. Electrochem. Sci.*, 6 (2011) 1981.
13. M.R. Ganjali, M. Hosseini, M. Pirali-Hamedani, H.A. Zamani, *Int. J. Electrochem. Sci.*, 6 (2011) 2808.
14. M.R. Ganjali, M. Rezapour, S.K. Torkestani, H. Rashedi, P. Norouzi, *Int. J. Electrochem. Sci.*, 6 (2011) 2323.
15. M.T. Montañés, R. Sánchez-Tovar, J. García-Antón, V. Pérez-Herranz, *Int. J. Electrochem. Sci.*, 5 (2010) 1934.
16. V.S.R. Channu, R. Holze, E.H. Walker, S.A. Wicker, R.R. Kalluru, Q.L. Williams, W. Walters, *Int. J. Electrochem. Sci.*, 5 (2010) 1355.
17. Z.H. Li, Q.L. Xia, L.L. Liu, G.T. Lei, Q.Z. Xiao, D.S. Gao, X.D. Zhou, *Electrochim. Acta*, 56 (2010) 804.
18. A. Lewandowski, A. Świdorska-Mocek, I. Acznik, *Electrochim. Acta*, 55 (2010) 1990.
19. G.H. Lane, A.S. Best, D.R. MacFarlane, M. Forsyth, P.M. Bayley, A.F. Hollenkamp, *Electrochim. Acta*, 55 (2010) 8947.
20. V. Lair, J. Sirieix-Plenet, L. Gaillon, C. Rizzi, A. Ringuede, *Electrochim. Acta*, 56 (2010) 784.
21. Y.L. Zhu, Y. Katayama, T. Miura, *Electrochim. Acta*, 55 (2010) 9019.
22. M.C. Tsai, D.X. Zhuang, P.Y. Chen, *Electrochim. Acta*, 55 (2010) 1019.
23. S. Zein El Abedin, P. Giridhar, P. Schwab, F. Endres, *Electrochem. Commun.*, 12 (2010) 1084.
24. A. Lisenkov, M.L. Zheludkevich, M.G.S. Ferreira, *Electrochem. Commun.*, 12 (2010) 729.
25. T.Y. Wu, M.H. Tsao, F.L. Chen, S.G. Su, C.W. Chang, H.P. Wang, Y.C. Lin, W.C. Ou-Yang, I.W. Sun, *Int. J. Mol. Sci.*, 11 (2010) 329.
26. T.Y. Wu, M.H. Tsao, F.L. Chen, S.G. Su, C.W. Chang, H.P. Wang, Y.C. Lin, I.W. Sun, *J. Iran Chem. Soc.*, 7 (2010) 707.

27. M.H. Tsao, T.Y. Wu, H.P. Wang, I.W. Sun, S.G. Su, Y.C. Lin, C.W. Chang, *Mater. Lett.*, 65 (2011) 583.
28. S.H. Jeon, A.R.S. Priya, E.J. Kang, K.J. Kim, *Electrochim. Acta*, 55 (2010) 5652.
29. T.Y. Wu, M.H. Tsao, S.G. Su, H.P. Wang, Y.C. Lin, F.L. Chen, C.W. Chang, I.W. Sun, *J. Braz. Chem. Soc.*, 22 (2011) 780.
30. G. Lakshminarayana, M. Nogami, *Electrochim. Acta*, 55 (2010) 1160.
31. K.K. Denshchikov, M.Y. Izmaylova, A.Z. Zhuk, Y.S. Vygodskii, V.T. Novikov, A.F. Gerasimov, *Electrochim. Acta*, 55 (2010) 7506.
32. R. Mysyk, E. Raymundo-Piñero, M. Anouti, D. Lemordant, F. Béguin. *Electrochem. Commun.*, 12 (2010) 414.
33. T.Y. Wu, L. Hao, C.W. Kuo, Y.C. Lin, S.G. Su, P.L. Kuo, I.W. Sun, *Int. J. Electrochem. Sci.*, 7 (2012) 2047.
34. T.Y. Wu, B.K. Chen, L. Hao, C.W. Kuo, I.W. Sun, *J. Taiwan Inst. Chem. Eng.*, 43 (2012) 313.
35. T.Y. Wu, I.W. Sun, S.T. Gung, B.K. Chen, H.P. Wang, S.G. Su, *J. Taiwan Inst. Chem. Eng.*, 43 (2012) 58.
36. S.Y. Ku, S.Y. Lu, *Int. J. Electrochem. Sci.*, 6 (2011) 5219.
37. T.Y. Wu, B.K. Chen, L. Hao, Y.C. Lin, H.P. Wang, C.W. Kuo, I.W. Sun, *Int. J. Mol. Sci.*, 12 (2011) 8750.
38. T.Y. Wu, B.K. Chen, L. Hao, Y.C. Peng, I.W. Sun, *Int. J. Mol. Sci.*, 12 (2011) 2598.
39. T.Y. Wu, I.W. Sun, S.T. Gung, B.K. Chen, H.P. Wang, S.G. Su, *J. Taiwan Inst. Chem. Eng.*, 42 (2011) 874.
40. T.Y. Wu, S.G. Su, S.T. Gung, M.W. Lin, Y.C. Lin, W.C. Ou-Yang, I.W. Sun, C.A. Lai, *J. Iran. Chem. Soc.*, 8 (2011) 149.
41. T.Y. Wu, S.G. Su, H.P. Wang, Y.C. Lin, S.T. Gung, M.W. Lin, I.W. Sun, *Electrochim. Acta*, 56 (2011) 3209.
42. T.Y. Wu, B.K. Chen, L. Hao, K.F. Lin, I.W. Sun, *J. Taiwan Inst. Chem. Eng.*, 42 (2011) 914.
43. T.Y. Wu, I.W. Sun, S.T. Gung, M.W. Lin, B.K. Chen, H.P. Wang, S.G. Su, *J. Taiwan Inst. Chem. Eng.*, 42 (2011) 513.
44. O.O. Okoturo, T.J. Vander Noot, *J. Electroanal. Chem.*, 568 (2004) 167.
45. T.Y. Wu, H.C. Wang, S.G. Su, S.T. Gung, M.W. Lin, C.B. Lin, *J. Taiwan Inst. Chem. Eng.*, 41 (2010) 315.
46. K. Liu, Y.X. Zhou, H.B. Han, S.S. Zhou, W.F. Feng, J. Nie, H. Li, X.J. Huang, M. Armand, Z.B. Zhou, *Electrochim. Acta*, 55 (2010) 7145.
47. T.Y. Wu, H.C. Wang, S.G. Su, S.T. Gung, M.W. Lin, C.B. Lin, *J. Chin. Chem. Soc.*, 57 (2010) 44.
48. H.B. Han, K. Liu, S.W. Feng, S.S. Zhou, W.F. Feng, J. Nie, H. Li, X.J. Huang, H. Matsumoto, M. Armand, Z.B. Zhou, *Electrochim. Acta*, 55 (2010) 7134.
49. T.Y. Wu, S.G. Su, Y.C. Lin, H.P. Wang, M.W. Lin, S.T. Gung, I.W. Sun, *Electrochim. Acta*, 56 (2010) 853.
50. A.B. Pereiro, A. Rodríguez, *J. Chem. Eng. Data*, 52 (2007) 600.
51. S. Himmler, S. Hörmann, R. Hal, P.S. Schulz, P. Wasserscheid. *Green Chem.*, 8 (2006) 887.
52. Z.-B. Zhou, H. Matsumoto, K. Tatsumi, *Chem. Eur. J.*, 11 (2005) 752.
53. J. Jacquemin, P. Husson, A.A.H. Padua, V. Majer, *Green Chem.*, 8 (2006) 172.
54. K.R. Seddon, A.S. Starck, M.J. Torres, ACS Symposium Series 901, Washington, DC, 2004.
55. P. Bonhote, A.P. Dias, N. Papageorgiou, K. Kalyanasundaram, M. Grätzel, *Inorg. Chem.*, 35 (1996) 1168.
56. W. Xu, E.I. Cooper, C.A. Angell, *J. Phys. Chem. B*, 107 (2003) 6170.
57. D.R. MacFarlane, M. Forsyth, E.I. Izgorodina, A.P. Abbott, G. Annat, K. Fraser, *Phys. Chem. Chem. Phys.*, 11 (2009) 4962.
58. N. Senda, Winmostar, version 3.78f (URL: <http://winmostar.com/>).
59. K. Liu, Y.X. Zhou, H.B. Han, S.S. Zhou, W.F. Feng, J. Nie, H. Li, X.J. Huang, M. Armand, Z.B.

Zhou, *Electrochim. Acta*, 55 (2010) 7145.

60. T.Y. Wu, S.G. Su, H.P. Wang, I.W. Sun, *Electrochem. Commun.*, 13 (2011) 237.

© 2012 by ESG (www.electrochemsci.org)